Pramāṇa, Vol. 22, No. 2, February 1984, pp. 79–88, © Printed in India.

Energy dependence of photon-induced L shell x-ray intensity ratios in Ta and W

K SHATENDRA*, K L ALLAWADHI and B S SOOD**

Department of Physics, Punjabi University, Patiala 147 002, India
* Present Address: Department of Physics, S A Jain College, Ambala 134 002, India
** Department of Physics, The Florida State University, Tallahassee, Florida 32306, USA

MS received 21 September 1983; revised 5 January 1984

Abstract. The L shell x-ray intensity ratios have been measured for the elements Ta and W by photoionization of L shell electrons in the photon energy region $14 \leqslant E \leqslant 44$ keV. The experimental results are compared with those calculated at the photon energies used in the present measurements. The measured values show fairly good agreement with the calculated values within the experimental uncertainties.

Keywords. X-ray intensities; fluorescent x-rays; photoionization; tantalum; tungsten.

1. Introduction

The phenomenon of atomic inner shell excitation/ionization by photons, electrons, protons and other heavy charged particles has been investigated by many workers, with a view to understand the various processes of the interaction of photons/charged particles with atomic electrons. The various physical parameters involved in the investigation are shell/subshell ionization cross-sections; fluorescence and Auger yields; Coster-Kronig transition probabilities and relative x-ray and electron intensities. While the K shell parameters for various elements have been extensively investigated, the measurements for the L and higher shell parameters are limited and confined mostly to the charged particle interactions.

We have measured the intensity ratios $I(L_{\alpha+l})/I(L_\beta)$ and $I(L_{\alpha+l})/I(L_\gamma)$ of the L shell x-rays following the photoelectric interaction of photons of various energies in the range $14 \leqslant E \leqslant 44$ keV in Ta and W. The use of the photoelectric interaction for the selective ionization of the L shell electrons allows the determination of the distribution of the initial vacancies among the three L subshells before the Coster-Kronig transitions, with confidence, since reliable values of L subshell photoelectric cross-sections are now available (Pratt *et al* 1973; Scofield 1973). The final distribution of vacancies after the Coster-Kronig transitions is evaluated using the values of the Coster-Kronig transition probabilities and subshell fluorescence yields available in literature and compared with the present experimental values. The method of measurement and the results are reported in this paper.

2. Experimental set-up and method of measurement

The experimental set-up is shown in figure 1. The radiation from a radioactive source ^{241}Am of strength $\sim$ 1 Curie are collimated to fall on primary targets of Rb, Y, Zr, Nb,

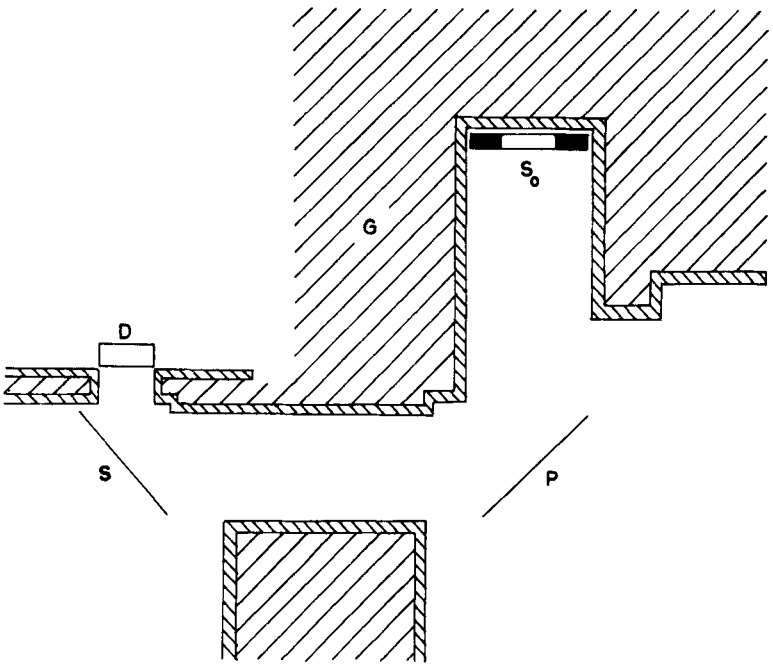

Figure 1. Experimental set-up for the measurement of L x-rays intensity ratios; S_0 – ^{241}Am source, P—primary target, S—secondary target, D—detector, G—graded shielding of Pb, Fe and Al.

Mo, Ag, In, Sn, I, Ba, La, Ce, Sm and Gd. The radiation emitted from the primary targets are collimated to fall on the secondary metallic targets of Ta and W of diameter 4 cm each and thicknesses 13·2 and 19·3 mg/cm^2 respectively. The L shell fluorescent x-rays emitted from the secondary target are analyzed with a Si(Li) detector of active area $\sim$ 200 mm^2 and sensitive depth 5 mm, coupled to ND 600 multichannel analyzer having energy resolution $\sim$ 240 eV at 5·9 keV. The shielding is so arranged that the source can see directly the primary target only. The primary and secondary targets can see each other. In addition to 59·57 keV gamma rays, Np L x-rays, 26 keV and some high energy gamma rays of very low intensity are also emitted from ^{241}Am source (Radiochemical Centre, Amersham, Nuclide Index 1977/78). The high energy gamma rays are not of much significance in the present experiment because of their very low intensities, small scattering cross-sections for the primary target elements and small L shell ionization cross-sections for the secondary target elements at the scattered energies. However, great care has to be exercised to avoid the interference from the Np L x-rays and 26 keV gamma rays because of their large scattering and ionization cross-sections. These are almost completely (more than 99·99 %) filtered out from the beam of radiation incident on the primary target by using a graded filter of Pb, Cu, and Al of thickness 0·15, 0·1 and 1 mm respectively. The radiations which are emitted from the primary target and made to fall on the secondary target consist of the two main components. The first component contains mostly K conversion x-rays characteristic of the primary target element produced almost wholly by the photoelectric interaction of 59·57 keV gamma rays. The L conversion x-rays in very low intensity are also

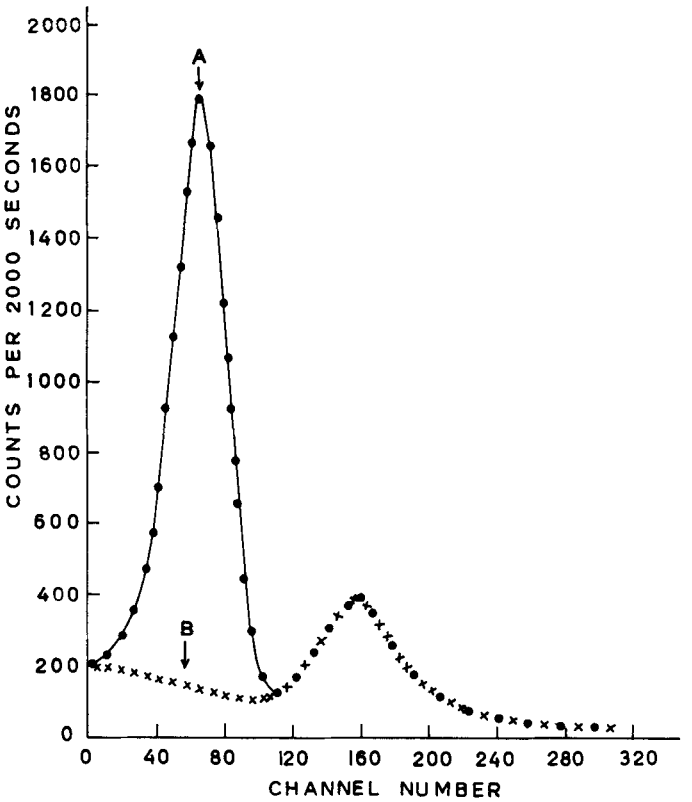

Figure 2. Primary spectra recorded with a 1·75 × 2″ thick NaI (Tl) crystal spectrometer placed at secondary target position when the targets were irradiated with 59·57 keV gamma rays from ^{241}Am; A—Sn primary target, B—Equivalent Al primary target. The first intense peak is due to Tin K x-rays and the second peak is due to the scattered radiation.

emitted, but their energies are such that they are unable to excite the secondary L x-rays and are therefore not significant in the present investigation. The second component consists of coherent and incoherent scattering of 59·57 keV gamma rays from primary target which is much smaller than conversion x-rays and is taken into account by using an equivalent Al target.

The spectra of the radiation emitted from the primary target elements and equivalent Al target are matched to give the same scattering by adjusting the thickness of the equivalent Al target. Typical results are shown in figure 2 where A and B represent the spectral distribution of radiation emitted with Sn and equivalent Al primary targets respectively. The scattering of 59·57 keV gamma rays is seen to be very nearly same from both the targets and A minus B spectrum consists almost entirely of K conversion x-rays of the primary target element Sn. The experimental conditions are thus so arranged that the secondary targets are irradiated only by the K conversion x-rays characteristic of primary target elements of weighted mean energies $13{\cdot}596 \leqslant E \leqslant 43{\cdot}946$ keV. The primary target elements with atomic number $37 \leqslant Z \leqslant 64$ are so chosen that the energies of all the components of their external conversion K x-rays are lower than the threshold energy for K shell but higher than the threshold energy of the L_I subshell of the elements of the secondary target. Therefore in the secondary target

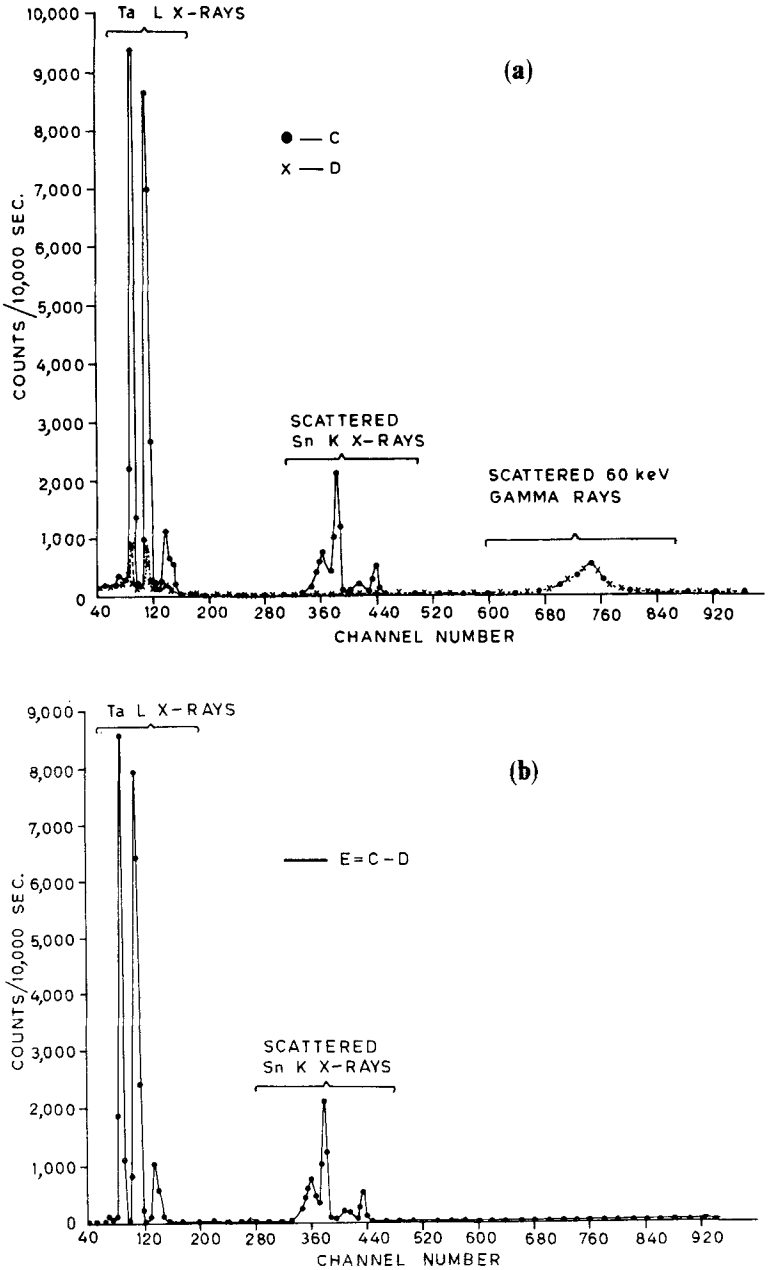

Figure 3 a. Secondary target spectra recorded with Si(Li) low energy photon spectrometer; C-Sn primary and Ta secondary; D-Equivalent Al primary and Ta secondary. **b.** spectrum $E = C\text{-}D$.

the K shell is not ionized but all the three subshells of the L shell are ionized. The distribution of the vacancies produced in the L shell is not disturbed due to the shift of the electrons from L to K shell. The relative initial vacancy can thus be calculated from the relative photo-ionization cross-sections. Typical secondary target spectra are shown in figure 3 where C and D represent the spectral distribution of radiation emitted from Ta secondary target when it is irradiated with radiation from Sn and equivalent Al-primary targets respectively. The spectrum $E = C\text{-}D$ between the channels ~ 60 to ~ 180 represents the L x-rays produced by the interaction of Sn K x-rays with Ta L-shell electrons. The other peaks are due to Sn K x-rays scattered from Ta target. It is seen to consist of resolved peaks corresponding to $L_{\alpha+l}$, L_β and L_γ group of lines; L_l peak is not completely resolved from the L_α peak due to the limited resolution of the available spectrometer. The number of L x-rays counted under any of the observed peak is due to the transitions from M, N and higher subshells to any of the three subshells depending upon their energies and selection rules. The intensity ratio of the x-rays $I(L_i)/I(L_j)$ under the peaks corresponding to groups of lines L_i and L_j is related to the ratio of number of counts per unit time $N(L_i)/N(L_j)$, contained in the areas under the respective peaks through the relation

$$\frac{I(L_i)}{I(L_j)} = \frac{N(L_i)}{N(L_j)} \frac{\beta(L_j)}{\beta(L_i)} \frac{\varepsilon(L_j)}{\varepsilon(L_i)}, \tag{1}$$

where $i = \alpha + l; \quad j = \beta, \gamma$

where $\beta(L_i)$ is the self-absorption correction factor that accounts for the absorption in the target of the incident primary K x-rays and the emitted secondary L x-rays in the L_i group; $\varepsilon(L_i)$ is the effective efficiency for the detection of L x-rays in the L_i group under the peak in the present geometry of the experiment. The $N(L_i)/N(L_j)$ values are determined by measuring the areas under the corresponding peaks. The $\beta(L_j)/\beta(L_i)$ values are calculated using the absorption coefficients at the incident and emergent x-ray energies in the target materials from the tables of Veigele (1973). Since both the incident and the emergent x-rays consist of a number of components, the procedure for calculation of β described earlier is followed (Arora *et al* 1981). The values of the overall effective efficiencies to detect x-rays of energies in the range $6 \leqslant E \leqslant 32$ keV are determined in a separate comparison experiment. Targets having areas of cross-section similar to the secondary targets used in the main experiment but of atomic numbers $26 \leqslant Z \leqslant 56$ were irradiated in the same geometry and the fluorescent K x-rays emitted from them were counted. The effective detection efficiency is determined in terms of the K shell photoelectric cross-section and fluorescence yields as explained in detail earlier (Allawadhi *et al* 1978). The effective overall detection efficiency at different energies is shown in figure 4. The values of the effective efficiency to detect x-rays under different peaks are taken from figure 4. The energies of the various peaks are taken to be the weighted mean energies of the various components incident under the corresponding peaks (Storm and Israel 1970). The overall error in the determination of $\varepsilon(L_j)/\varepsilon(L_i)$ is $\sim 5\%$. It may be mentioned that standard photon sources in the energy region of interest in the present measurements for the efficiency calibration of the detector are not available. The present method is therefore used for the efficiency calibration of the detector.

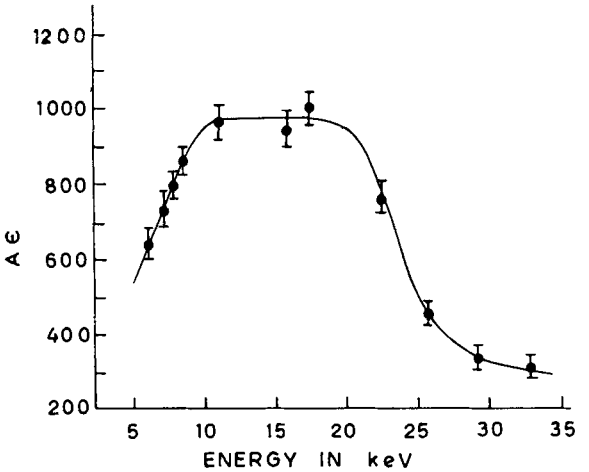

Figure 4. Effective efficiency calibration curve for (200 mm^2 × 5 mm) Si(Li) detector.

3. Results and discussion

The values of the intensity ratios $I(L_{\alpha+l})/I(L_\beta)$ and $I(L_{\alpha+l})/I(L_\gamma)$ as determined experimentally using (1) are given in table 1 and figures 5 and 6 for Ta and W respectively. The errors shown in the experimental values vary from 10 to 12% and are due to the counting statistics and uncertainties involved in the other quantities. The details of error break-up are given in table 2. Since no other experimental measurements using photoionization as mode of vacancy production are available, the present results are compared with the values calculated using the intensity relations (Close *et al* 1973)

$$I(L_{\alpha+l}) = \{N_1 f_{13} + N_1 f_{12} f_{23} + N_2 f_{23} + N_3\}\,\omega_3 (F_{3\alpha} + F_{3l}), \tag{2}$$

$$I(L_\beta) = N_1 \omega_1 F_{1\beta} + \{N_2 + N_1 f_{12}\}\,\omega_2 F_{2\beta} + \{N_1 f_{13} + N_1 f_{12} f_{23} + N_2 f_{23} + N_3\}\,\omega_3 F_{3\beta}, \tag{3}$$

$$I(L_\gamma) = N_1 \omega_1 F_{1\gamma} + \{N_2 + N_1 f_{12}\}\,\omega_2 F_{2\gamma}, \tag{4}$$

N_1, N_2 and N_3 are the relative vacancy numbers in the subshells L_I, L_{II} and L_{III} respectively produced through photoionization before the Coster-Kronig transitions; f_{12}, f_{13} and f_{23} are the various Coster-Kronig transition probabilities; ω_1, ω_2 and ω_3 are the L subshell fluorescence yields; $F_{3\beta}$ defines the fraction of radiative transitions in the L_β group of x-rays resulting from the filling of a vacancy in the L_{III} subshell. All other F's are similarly defined. The N_1, N_2 and N_3 values are determined from the interpolation of the L subshell photoionization cross-sections values calculated by Scofield (1973) at the photon energies used in the present measurements. The Coster-Kronig transition probabilities values and the subshell fluorescence yields are taken from the calculations of Chen and Crasemann (1981) and the semi-empirical data compiled by Krause *et al* (1978) using the technique of employing the best fit to all the available data of different workers. The F values were taken from the calculations of Scofield (1969). The relative intensities calculated from (2)–(4) are compared with the

Table 1. Experimental values of L x-ray intensity ratios measured at various K x-ray energies for W and Ta compared with theoretically calculated values using parameters ω and f' s from Krause *et al* (1978) and Chen and Crasemann (1981).

		W				Ta			
		$I(L_{\alpha+l})/I(L_\beta)$		$I(L_{\alpha+l})/I(L_\gamma)$		$I(L_{\alpha+l})/I(L_\beta)$		$I(L_{\alpha+l})/I(L_\gamma)$	
Z	Weighted average K energy (keV)	Present experiment	Theory	Present experiment	Theory	Present experiment	Theory	Present experiment	Theory
37	13·596	1·16 ± 0·12	1·03* 1·02	6·65 ± 0·73	5·87* 5·73	1·15 ± 0·13	1·02	6·53 ± 0·72	5·91
39	15·200	1·11 ± 0·10	1·00* 0·99	5·46 ± 0·60	5·64* 5·48	1·19 ± 0·13	0·98	7·06 ± 0·73	5·64
40	16·035	1·14 ± 0·11	0·99* 0·97	6·51 ± 0·61	5·53* 5·37	1·19 ± 0·12	0·97	6·03 ± 0·71	5·53
41	16·896	1·11 ± 0·10	0·97* 0·96	5·73 ± 0·72	5·44* 5·26	1·13 ± 0·11	0·96	6·33 ± 0·71	5·42
42	17·781	1·11 ± 0·11	0·96* 0·94	6·21 ± 0·79	5·34* 5·16	1·12 ± 0·13	0·95	6·02 ± 0·70	5·32
47	22·581	1·09 ± 0·12	0·91* 0·88	5·34 ± 0·69	4·95* 4·70	1·06 ± 0·11	0·89	5·60 ± 0·65	4·85
49	24·681	1·04 ± 0·10	0·89* 0·86	5·15 ± 0·62	4·77* 4·54	1·06 ± 0·12	0·86	5·61 ± 0·69	4·68
50	25·770	1·03 ± 0·11	0·88* 0·85	4·91 ± 0·58	4·70* 4·46	1·02 ± 0·12	0·85	5·71 ± 0·60	4·60
53	29·208	1·00 ± 0·12	0·85* 0·82	4·98 ± 0·53	4·50* 4·24	1·02 ± 0·12	0·84	5·48 ± 0·61	4·38
56	32·890	0·98 ± 0·12	0·82* 0·78	4·92 ± 0·64	4·27* 3·99	0·95 ± 0·11	0·80	5·11 ± 0·61	4·18
57	34·169	0·94 ± 0·13	0·82* 0·78	5·94 ± 0·70	4·27* 3·99	0·91 ± 0·13	0·79	4·64 ± 0·62	4·12
58	35·478	0·90 ± 0·11	0·81* 0·77	5·18 ± 0·67	4·22* 3·94	0·94 ± 0·12	0·78	6·35 ± 0·63	4·06
62	41·006	0·92 ± 0·12	0·79* 0·75	4·85 ± 0·62	4·03* 3·73	0·86 ± 0·12	0·75	4·97 ± 0·60	3·85
64	43·949	0·95 ± 0·11	0·78* 0·73	4·48 ± 0·49	3·94* 3·63	0·96 ± 0·11	0·74	6·70 ± 0·62	3·75

* Values calculated using the values of ω and f's from Chen and Crasemann (1981).

Table 2. Uncertainties involved in the quantities used to determine intensity ratios $I(L_{\alpha+l})/I(L_\beta)$ and $I(L_{\alpha+l})/I(L_\gamma)$ from equation 1.

Quantity	Nature of uncertainty	Uncertainty
$N(L_i)$ and $N(L_j)$	Statistical	1%
$\beta(L_i)$ and $\beta(L_j)$	Due to errors in the absorption coefficients at incident and emitted photon energies etc.	4–5%
$\varepsilon(L_i)$ and $\varepsilon(L_j)$	Statistical and due to K-shell photoelectric cross-sections, fluorescence yields and absorption coefficients, etc.	5–6%

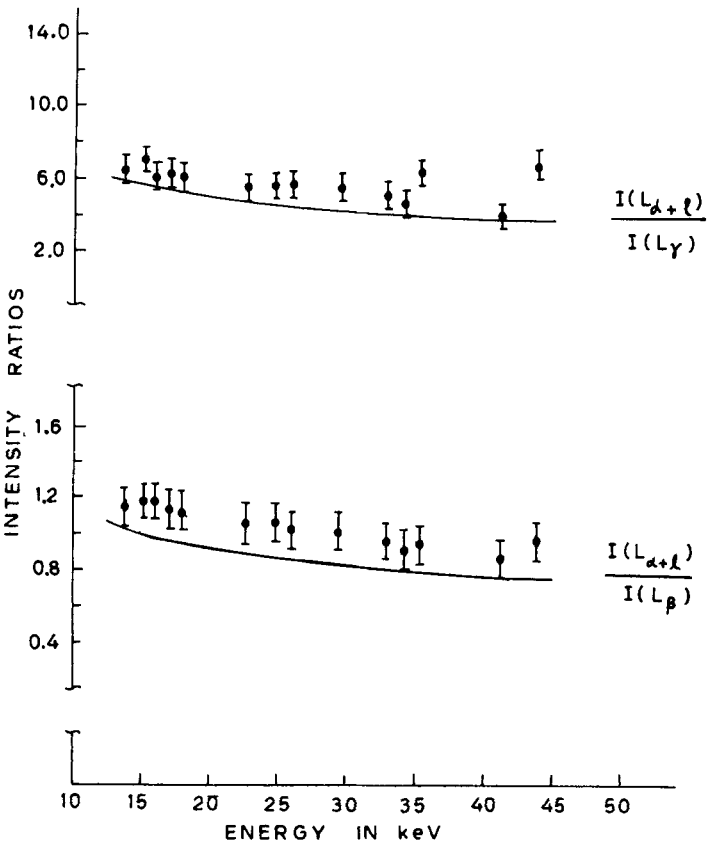

Figure 5. L x-ray intensity ratios for Ta measured at various incident photon energies (●) compared with the calculated values using the parameters ω and f's from Krause *et al* (1978) (——).

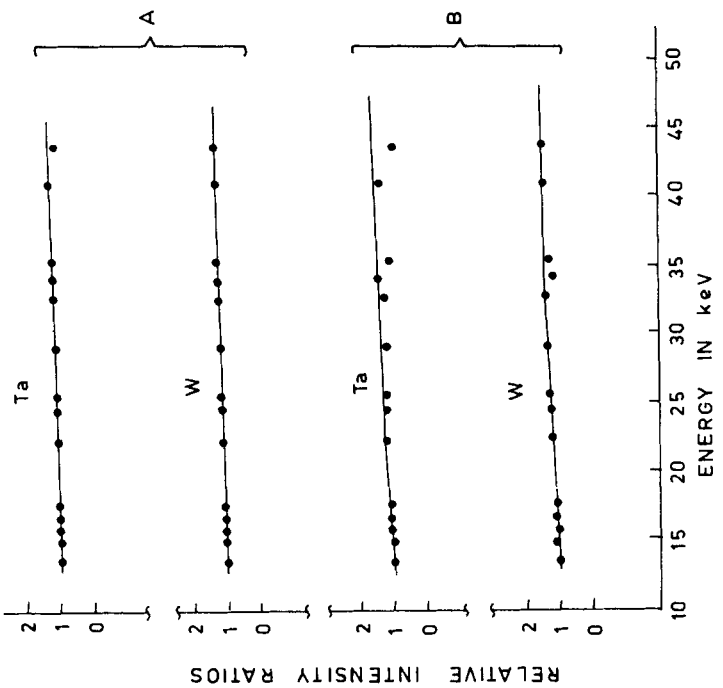

Figure 7. Plot of relative-intensity ratios *vs* incident photon energy.

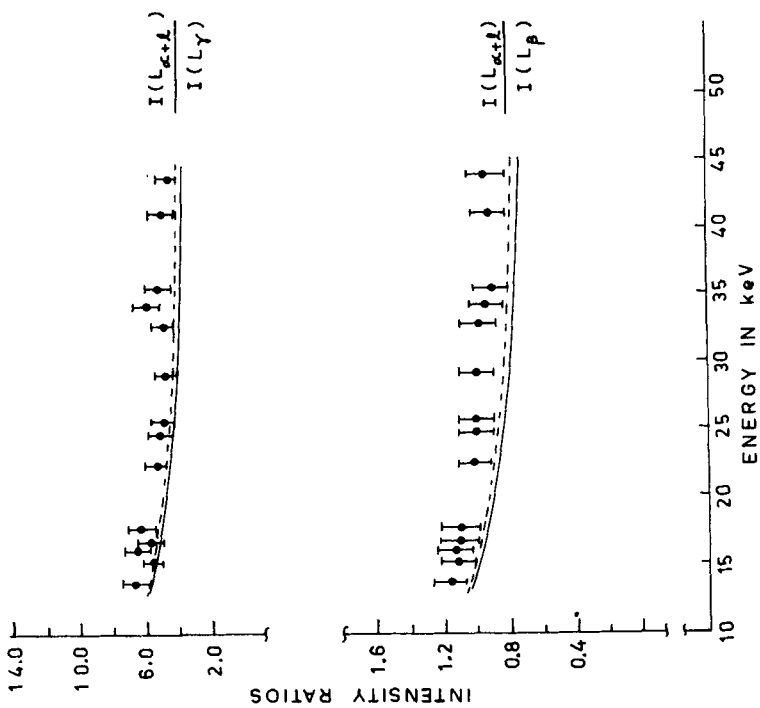

Figure 6. *L* x-ray intensity ratios for W measured at various incident photon energies (●) compared with the calculated values using the parameters ω and f's from Krause *et al* (1978) (——), Chen and Crasemann (1981) (– – – –).

present results in table 1 and figures 5 and 6. The experimental values of the ratios are found to be 10–15% higher than the calculated values. This discrepancy may be ascribed to either the under-estimation of the calculated values or over-determination of the experimental values. Since experimental values depend only on the determination of the ratios of three physical quantities, over-estimation of the results upto 10–15% is unlikely, whereas the knowledge of the Coster-Kronig transition probabilities and the L subshell fluorescence yields needed in the calculations of the intensity ratios is inadequate as yet. The above discrepancy should be reduced if relative instead of absolute values of intensity ratios are compared with theory. A comparison of the experimental and calculated intensity ratios relative to the ratio at 13·596 keV is shown in figure 7. The agreement between experiment and theory, as expected, is found to be good.

Acknowledgement

Financial assistance from UGC is gratefully acknowledged.

References

Allawadhi K L, Arora S K and Sood B S 1978 *Pramana* **10** 511
Arora S K, Allawadhi K L and Sood B S 1981 *J. Phys.* **B14** 1423
Chen M H and Crasemann B 1981 *Phys. Rev.* **A24** 177
Close D A, Bearse R C, Malanify J J and Umberger J J 1973 *Phys. Rev.* **A8** 1873
Krause M O, Nestor Jr C W, Spark Jr C J and Ricci E 1978 Oak Ridge National Laboratory, Report No. 5399
Pratt R H, Ron A and Tseng H K 1973 *Rev. Mod. Phys.* **45** 273
Radiochemical Centre, Amersham, Nuclide Index 1977/78
Scofield J H 1969 *Phys. Rev.* **A179** 9
Scofield J H 1973 Lawrence Livermore Laboratory, Report No. 51326
Storm E and Israel I 1970 *Nucl. Data Tables* **A7** 565
Viegele W J 1973 *At. Data Tables* **5** 51